Application of MRI to study disease progression in multiple sclerosis

by

Adrian Wu

A THESIS SUBMITTED IN PARTIAL FULFILLMENT OF
THE REQUIREMENTS FOR THE DEGREE OF

BACHELOR OF SCIENCE, HONOURS PHYSICS

in

The Faculty of Science

(Physics and Astronomy)

THE UNIVERSITY OF BRITISH COLUMBIA

(Vancouver)

July 2024

The following individuals certify that they have read, and recommend to the Faculty of Science for acceptance, the thesis entitled:

Application of MRI to study disease progression in multiple sclerosis

submitted by **Adrian Wu** in partial fulfillment of the requirements for the degree of **BACHELOR OF SCIENCE, HONOURS PHYSICS** in **Physics and Astronomy**

Examining Committee:

Supervisor: Dr. Shannon Kolind

Additional Examiner: Sharada Balaji

Abstract

Multiple Sclerosis (MS) is a chronic autoimmune and neurodegenerative disorder that affects the central nervous system and may lead to permanent disability. Advanced, quantitative MRI data for a large cohort of people living with MS from across Canada has been collected. The proposed project will involve using this data to determine factors impacting disease progression using tractometry, myelin water imaging, and diffusion tensor imaging. We intend to track how different MRI measures vary along different white matter tracts which will help reveal how, where, and when myelin and axons are damaged. A better understanding of the underlying mechanisms will aid in creating new treatments that can alter the course of disease progression, and will greatly benefit individuals with MS.

Lay Summary

Multiple Sclerosis (MS) is a complex disease affecting the central nervous system, leading to long-term disability. Despite extensive research, effective treatments to halt disease progression remain elusive. Our research utilizes data collected from the Canadian Prospective Cohort Study to Understand Progression in MS (CanProCo), which includes detailed MRI scans from a large cohort of MS patients across Canada. One step towards understanding disease progression is categorizing lesions in the MS brain. Current categorizations are based on histology, which requires post-mortem tissue staining. We wish to classify lesions in vivo using quantitative MRI. In this thesis, we show there are three categories lesions belong to. Lesions may either affect primarily myelin water fraction (MWF), fractional anisotropy (FA), or both. This suggests certain areas may contain more myelin or axonal damage.

Preface

The content of this thesis is original unpublished work by the author. The idea for this study came about through discussions with the author's supervisor, Dr. Kolind. All necessary python scripts, as well as the resulting plots and data were created by the author. Data processing scripts were created by Sharada Balaji, but adapted for use in this project. Processed quantitative maps were created by Poljanka Johnson. Individual techniques and methods used but not developed by the author have been cited where appropriate.

Table of Contents

Abstract . . . ii

Lay Summary . . . iii

Preface . . . iv

Table of Contents . . . v

List of Tables . . . vi

List of Figures . . . vii

Acknowledgements . . . ix

1 Introduction . . . 1

2 Theory . . . 2
- 2.1 Magnetic Resonance Imaging . . . 2
- 2.2 Myelin Water Imaging . . . 3
- 2.3 Diffusion Tensor Imaging . . . 5
- 2.4 Tractography . . . 6

3 Methods . . . 7
- 3.1 Data used . . . 7
- 3.2 Initial registration . . . 7
- 3.3 Tract atlas . . . 8
- 3.4 Tractometry for MS . . . 10
- 3.5 Lesion identification and classification . . . 10

4 Results . . . 13
- 4.1 Lesion categorization . . . 13
- 4.2 Statistical analysis . . . 15

5 Analysis and Discussion . . . 20

6 Conclusion . . . 22

Bibliography . . . 23

List of Tables

3.1 Categorization criteria 11

4.1 Lesion category summary 13
4.2 ANOVA results for MWF and FA 16
4.3 Tukey results for MWF 19
4.4 Tukey results for FA 19

List of Figures

2.1 The image above shows the precession of a hydrogen nuclei with (a) Only a uniform field, B_0, is applied. All nuclei precess at the same frequency. (b) A gradient field, B_1, with gradient along the x-direction is applied. The nuclei resonate and precess faster along the x-direction. Precession frequency depends on position along the x-axis. [1] 3

2.2 The image above shows the T_2 distribution from human white matter in different locations. The signal from myelin has a shorter T_2 decay time than the signal from intra and extracellular water, and its peak appears at a smaller T_2 time on a T_2 distribution. [2] 4

2.3 Myelin Water Fraction map of a healthy individual. [2] 4

2.4 The illustration on the left depicts myelinated axons, overlaid with the x, y, and z axes of the MRI scanner. On the right, the motion of water within the bundle of axons is represented as an ellipsoid. The diffusion tensor is diagonalized to obtain the eigenvectors $\Sigma_1, \Sigma_2, \Sigma_3$ and corresponding eigenvalues $\lambda_1, \lambda_2, \lambda_3$. The orientation of the ellipsoid is defined by three eigenvectors; the longest axis is the side with the highest diffusivity and thus eigenvalue. Diffusion is limited in directions perpendicular to the length of the axon (λ_2, λ_3), and is greater in the direction parallel to the length of the fiber (λ_1). [3] 5

3.1 FLAIR, FA, and MWF maps for a healthy control and MS brain illustrates the power of image registration for lesion identification. The lesion in the MS brain is indicated by the red arrow. Lesions that appear as bright spots on a FLAIR may also appear on FA and MWF maps as damage in those same regions. Damage levels may vary subject to subject, and even lesion to lesion in the same brain. . 9

3.2 Tract profiles of 4 RRMS subjects for portions of the corpus callosum (CC), where red boxes indicate tracts with lesions found on them. This allows us to categorize lesions based on decreases in MWF or FA, as well as compare lesion tracts to tracts where we did not find lesions. 11

3.3 Tract profile for a PPMS subject showing MWF and FA values along the tract. FA is plotted in orange and MWF in blue, with the healthy means shown in the corresponding shaded regions. The orange and blue arrows illustrate how mean average percent error (MAPE) is calculated by taking the absolute value of the difference between the tract profile and healthy mean values along the tract, then averaging. 12

4.1 Tract profiles for the three categories we identified. (a) MWF-type lesion shows MWF significantly below the healthy average values across the whole tract, and may be primarily myelin damage driven. (b) FA-type lesions show FA decreases in the middle of the tract and may be primarily axon damage driven. (c) Both-type lesions show MWF and FA decreases across the tract, and show signs of damage in both myelin and axon integrity. 14
4.2 White matter tract coloured by MWF and FA values of a MWF-type lesion in a RRMS subject. The lesion is indicated by the white arrow. MWF is decreased compared to the healthy control in the region around the lesion. Parts of the tract not touching the lesion also show signs of decreased myelin, suggesting there may be downstream effects. FA values in the MS tract are comparable to the healthy control. 15
4.3 White matter tract coloured by MWF and FA values of an FA-type lesion in a RRMS subject. The lesion is indicated by the white arrow. A decrease in FA can be seen in the FA tract near the lesion on the right, and FA appears to be lower overall. MWF appears to be unaffected and similar to the healthy control. 16
4.4 White matter tract coloured by MWF and FA values of a Both-type lesion in a RRMS subject. The lesion is indicated by the white arrow. MWF is significantly decreased near the lesion on the right in the MS tract, also showing signs of potential downstream damage. FA is lower near the branches of this tract compared to the healthy control, indicated by the darker orange/red colouring. 17
4.5 Box plots grouped by subject types for various metrics. (a) MWF MPE box plot. (b) MWF MAPE box plot (c) MWF RMS box plot (d) FA MPE box plot (e) FA MAPE box plot (f) FA RMS box plot. All metrics showed statistically significant differences between the HC and the other groups. No metric showed statistically significant differences between RRMs, PPMS, or RIS. It appears RIS has much larger variance in FA damage compared to MWF damage, and is consistent across all three metrics. Similarly, PPMS shows larger variance in MWF than in FA. 18

Acknowledgements

I would like to thank my supervisor Dr. Shannon Kolind for the opportunity to work on this project and for her ongoing guidance. Thank you to Sharada Balaji for the extensive support and whose knowledge helped me better understand MS imaging techniques. I would also like to thank Poljanka Johnson for creating the processed quantitative maps. I am grateful to all the researchers and participants who made CanProCo possible with all their efforts.

Chapter 1

Introduction

Multiple sclerosis (MS) is a chronic inflammatory demyelinating disease affecting the central nervous system (CNS). It is the most common inflammatory neurological disease in young adults, with over 2 million prevalent cases in 2016.[4] This inflammation gives rise to focal lesions in the gray and white matter; a diagnostic hallmark of this disease. This inflammation can also drive tissue injury, inducing varying degrees of myelin and axonal damage across the brain. Myelin and axon damage can vary greatly patient to patient, and even lesion to lesion. [5]

Few treatments currently exist that substantially modify the course of the clinical progression of MS. There has been considerable progress in the development of many more treatment options for one phenotype of MS, relapsing-remitting, but few treatments exist for progression in MS, which include phenotypes of the disease like primary progressive and secondary progressive. These possible treatments are unable to drastically alter the trajectory of disease progression, and only show modest efficacy. [4] The development of novel treatments and therapeutic agents that can target progression in MS requires that the determinants of clinical progression are identified and characterized. The Canadian Prospective Cohort Study to Understand Progression in MS (CanProCo) is an ongoing study aimed to evaluate a wide spectrum of factors associated with the clinical onset and rate of disease progression in MS, and to describe how these factors relate to one another to influence progression.[6]

Some of this MRI data is specific to myelin, and some to axonal integrity. While it is known MS results in myelin and axonal damage, it is unclear to what extent each is affected, and if other regions of the brain are also affected once one part is damaged. By comparing data on myelin content and axon integrity, we can investigate where and when myelin and axon damage occurs during disease progression. Techniques like myelin water imaging, tractometry, and diffusion tensor imaging allow us to track different MRI measures along white matter tracts over time. Tractometry is a tool we can use to assess MRI measures, such as myelin water fraction (MWF) and fractional anisotropy (FA), along white matter tracts.

This project aims to identify key mechanisms behind progression of MS using CanProCo imaging data. Looking at myelin and axon damage through the use of tractometry, myelin water imaging, and diffusion tensor imaging will help determine the driving forces behind disease progression. Longitudinal data is available and thus myelin and axon damage can be tracked over the course of the study to see how, where, and when damage occurs. Tracking this data will also allow for investigation into how lesions form, and if there are subtle, progressive alterations in tissue integrity. Another area of interest is to look at how lesion appearance and structural damage may affect connected areas of normal-appearing white matter (NAWM). [7]

A better understanding of the mechanisms and factors underlying disease progression is an area of great interest. The results from this project will aid the ongoing research focus on developing more effective and targeted therapies to modify the course of the disease, reduce relapses, and improve long-term outcomes for individuals with MS.

Chapter 2

Theory

2.1 Magnetic Resonance Imaging

Magnetic Resonance Imaging (MRI) is widely used in the medical field, primarily because it does not expose the patient to ionizing radiation and offers inherent adaptability. The absence of ionizing radiation makes MRI a relatively low-risk medical imaging method, suitable for research or clinical applications involving repeated scans and for imaging sensitive areas like the spine. The adaptability stems from the underlying physics of MRI, where adjustments to scan parameters enable a single MRI hardware system to capture a variety of different images. This versatility is achieved through intricate pulse sequences of magnetic field gradients applied to the subject, serving as the fundamental method for generating a measurable signal that is then reconstructed into an image. Researchers continuously modify scan parameters to develop imaging techniques that offer new and unique insights into the subject and the microstructure of underlying tissues, providing significant benefits to patients in clinical settings.

Nuclei that have an odd number of protons or neutrons possess an inherent nuclear spin and magnetic moment, which can be affected by magnetic fields. The signal in most MRI imaging, including that in this study, originates from hydrogen nuclei, primarily found in water molecules. They act as free protons. In the absence of an applied magnetic field, these spins are randomly oriented and result in a net zero spin and magnetic moment. When placed within a magnetic field, B_0, the spins align with or against the introduced field lines. In fact, only a small proportion more align with the field lines but are enough to create a measurable net magnetization. Once aligned to the magnetic field, external perturbations cause the nuclei to undergo precession around the B_0 axis. The frequency of this precession is governed by the equation for Larmor frequency.

$$\omega_0 = \gamma_0 B \tag{2.1}$$

In this equation, ω_0 represents the Larmor frequency in units of Hertz, γ_0 is the gyromagnetic ratio in Hertz per Tesla, and B is the strength of the magnetic field in Tesla.

Another oscillating magnetic field, B_1, is introduced and placed orthogonal to B_0. It will excite protons to a known Larmor frequency and cause proton precession at an angle to B_0. A proton's axis of precession relaxes back towards B_0 again once this RF pulse is turned off. This relaxation releases a signal which is measured and used to reconstruct an image. The signal alone does not contain information about where the signal comes from.

To spatially localize the MR signal, gradients are employed. These gradients introduce linear variations in static field strength and can be applied in any orthogonal direction (G_x, G_y, G_z). As a result, MR signals at various spatial positions can be differentiated, which facilitates three-dimensional image reconstruction. [8] [9] [10]

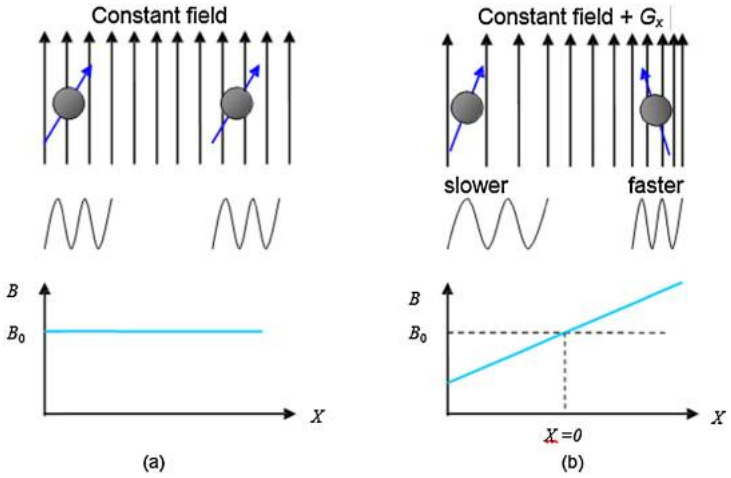

Figure 2.1: The image above shows the precession of a hydrogen nuclei with (a) Only a uniform field, B_0, is applied. All nuclei precess at the same frequency. (b) A gradient field, B_1, with gradient along the x-direction is applied. The nuclei resonate and precess faster along the x-direction. Precession frequency depends on position along the x-axis. [1]

2.2 Myelin Water Imaging

Myelin water imaging is a technique that aims to specifically visualize and quantify the water content associated with myelin in the central nervous system. Myelin is a fatty substance that forms a protective sheath around axons and is crucial for the efficient transmission of nerve impulses. The basic principle of myelin water imaging involves exploiting the different relaxation properties of water within myelin-rich regions compared to other tissues.

A signal originating from water within the layers of myelin, referred to as myelin water, can be distinguished from the signal of water in other parts of the nervous system. The ratio of the myelin water signal to the total water signal gives the myelin water fraction (MWF). Maps of myelin in the brain can be created by displaying the MWF as the color of a pixel. These myelin water images (MWI) show a strong correlation between myelin water and various myelin histological stains, like Luxol Fast Blue, in both the peripheral and central nervous systems. [11] [2]

The MR signal for Myelin Water Imaging comes from the protons of water molecules. Individual water molecules can experience very different microscopic environments due to interactions with their surroundings. A T_2 decay curve is a plot of the MR signal versus time. For a homogeneous sample, this decay curve is an exponentially decaying signal with rate constant $1/T_2$. The local environment determines the T_2 decay time for water. Myelin water typically has a T_2 time between 10 and 20ms. In comparison, intra and extracellular water has a decay time significantly beyond that, typically 40 to 200ms. Thus, a three dimension pixel, or voxel, that contains water in different environments will have a resulting T_2 decay curve that is the sum of exponential decays. The amplitudes will be proportional to the relative amounts of water in each environment. [2] [12]

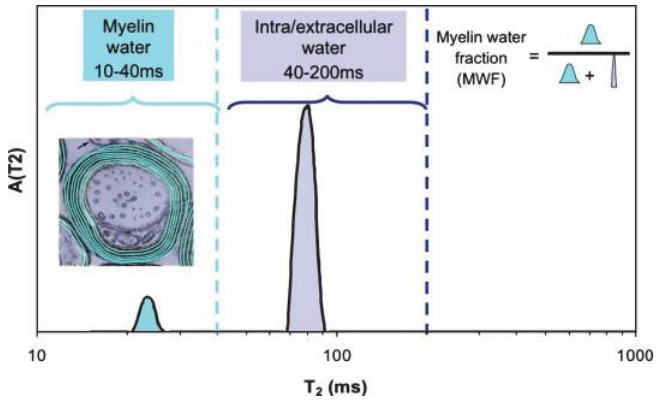

Figure 2.2: The image above shows the T_2 distribution from human white matter in different locations. The signal from myelin has a shorter T_2 decay time than the signal from intra and extracellular water, and its peak appears at a smaller T_2 time on a T_2 distribution. [2]

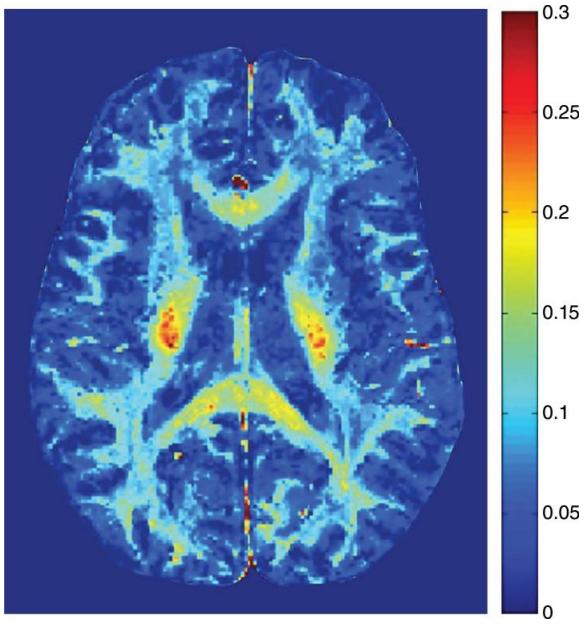

Figure 2.3: Myelin Water Fraction map of a healthy individual. [2]

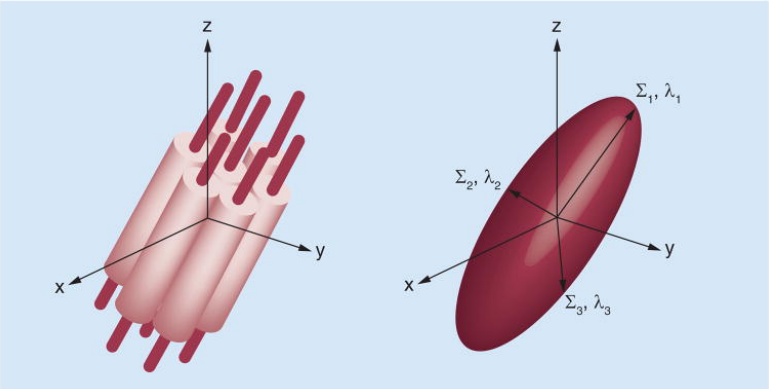

Figure 2.4: The illustration on the left depicts myelinated axons, overlaid with the x, y, and z axes of the MRI scanner. On the right, the motion of water within the bundle of axons is represented as an ellipsoid. The diffusion tensor is diagonalized to obtain the eigenvectors $\Sigma_1, \Sigma_2, \Sigma_3$ and corresponding eigenvalues $\lambda_1, \lambda_2, \lambda_3$. The orientation of the ellipsoid is defined by three eigenvectors; the longest axis is the side with the highest diffusivity and thus eigenvalue. Diffusion is limited in directions perpendicular to the length of the axon (λ_2, λ_3), and is greater in the direction parallel to the length of the fiber (λ_1). [3]

2.3 Diffusion Tensor Imaging

Diffusion Tensor Imaging (DTI) is a neuroimaging technique employed for the visualization and characterization of microstructural features within the brain. DTI captures and quantifies the directional movement of water molecules, which aligns with the orientation of neural fibers. The diffusion of water in biological tissues takes place within, outside, surrounding, and through cellular structures. Cellular membranes interact with water molecules, and may hinder their diffusion, causing them to take roundabout paths. This leads to a decreased mean squared displacement. In fibrous tissues, water diffusion is highly restricted and hindered perpendicular to the fibers, and is thus anisotropic. A 3×3 covariance matrix, called a diffusion tensor, can be used to describe this anisotropic diffusion:

$$D = \begin{pmatrix} D_{xx} & D_{xy} & D_{xz} \\ D_{yx} & D_{yy} & D_{yz} \\ D_{zx} & D_{zy} & D_{zz} \end{pmatrix} \tag{2.2}$$

where the diagonal elements describe the diffusion variances along the x, y, z axes. The off diagonal elements are covariance terms and are symmetric about the diagonal ($D_{ij} = D_{ji}$). Diagonalizing this matrix gives eigenvalues $\lambda_1, \lambda_2, \lambda_3$ and eigenvectors $\vec{v}_1, \vec{v}_2, \vec{v}_3$ which describe the direction and diffusivity along the axes of principle diffusion. When the eigenvalues are nearly equal, diffusion is "isotropic," and when they are significantly different in magnitude, diffusion is "anisotropic." Axial diffusivity (AD) is the measure of the amount of diffusion along the main axis of diffusion. In other words, it is the largest eigenvalue, and most diffusion will occur in the direction of this eigenvector.

One measure of the diffusion tensor is the mean diffusivity, MD, also known as the "apparent diffusion coefficient." It is a measure of the magnitude of diffusion and is rotationally invariant. It is defined as the trace of the diffusion tensor divided by 3, or simply average of the eigenvalues (Tr/3).

Another invariant measure is Fractional Anisotropy (FA). It provides insights into microstructural integrity. In the context of MS, FA serves as a crucial indicator for detecting demyelination and assessing axonal damage. Axon bundles typically have high FA whereas gray matter has low FA; with axon damage, one would expect to see reduced FA in those areas. FA is defined as:

$$\mathrm{FA} = \sqrt{\frac{(\lambda_1 - \mathrm{MD})^2 + (\lambda_2 - \mathrm{MD})^2 + (\lambda_3 - \mathrm{MD})^2}{2(\lambda_1^2 + \lambda_2^2 + \lambda_3^2)}} \tag{2.3}$$

To acquire an image using DTI, the alignment of proton spins is crucial for generating a strong signal in an MRI image. Initially, the spins must be in phase to produce a bright signal. A gradient magnetic field is then employed, causing spin dephasing. After some time t, an opposite gradient is applied, bringing the spins back into phase. For stationary particles, the gradient pulses cancel out perfectly, and the signal is maximally coherent. However, if molecules move during t, the second gradient application may fail to bring them back into phase. This resulting net phase difference will be proportional to the distance travelled. This process is repeated in various directions, yielding the three-dimensional diffusion tensor. [13] [14] [3]

2.4 Tractography

Fiber segmentation aids in the profiling of healthy brains and can identify areas containing abnormalities in the morphology of diseased brains via detailed analysis of individual white matter tracts.

Tractography is a technique in neuroimaging that involves mapping and visualizing the pathways of nerve fibers within the brain. Primarily utilized in conjunction with diffusion tensor imaging (DTI), tractography allows researchers and clinicians to create detailed three-dimensional representations of white matter tracts, which are bundles of nerve fibers responsible for transmitting signals between different regions of the brain. By tracking the directional movement of water molecules along these nerve fibers, tractography provides valuable insights into the structural connectivity of the brain.

The TractSeg library will be used to perform tractography in this project. It involves the automated analysis of white matter fiber tracts in the brain. TractSeg is a computational method to segment white matter tracts based on fiber orientation distribution (FOD) peaks. TractSeg receives three principal fiber directions per voxel as input, and demonstrates robustness, achieving accurate results even in areas where reference tracts are incomplete. This condensed representation of the input data allows various MRI acquisition methods to work with TractSeg. [15]

Tractography describes the process of creating the tracts whereas tractometry refers to tract profiling. With tractometry, variation along the tract is measured. Once a tract is created the final step is to retrieve the tract profile. Nodes are obtained by resampling along the tract, like mentioned above. Then the average value of a diffusion-derived scalar, such as FA or MD, is determined for each node. The values can then be summarized by weighing contributions from each fiber in a group based on how much its trajectory differs from the rest. [16]

Chapter 3

Methods

Data has been collected as part of the CanProCo study and will be used. The study employs a prospective, observational, cohort design with specialized investigators from diverse backgrounds. It involves 1000 participants diagnosed with radiologically isolated syndrome, relapsing-remitting MS, or primary progressive MS within 10-15 years of onset. The research spans across five academic MS centers in Canada, conducting detailed clinical evaluations annually over a 5-year period. A subset of 500 participants within 5-10 years of disease onset undergoes in-depth assessments, including the collection of blood, cerebrospinal fluid, and MRI scans. The investigation aims to comprehensively evaluate factors contributing to MS progression from various perspectives, encompassing biological measures such as RNA sequencing, MRI microstructural assessments, and micro/macro environmental factors.

3.1 Data used

From CanProCo, a subset of the main study data will be used; it contains 10 healthy controls 13 radiologically isolated syndrome (RIS), 15 relapsing-remitting MS (RRMS), and 11 primary-progressive MS (PPMS). All data was collected from Vancouver and only baseline data (month 0) will be used. MWI data in CanProCo was acquired using a 3D GRASE sequence with 48 echoes, TE = 8 ms, $1 \times 2 \times 5$ mm voxels, and a 6 minute scan. This allows changes in myelin in lesions and normal appearing white matter to be detected by calculating MWF. DTI data was acquired in 30 directions, $1.7 \times 1.7 \times 1.7$ mm isotropic voxels, TR/TE = 4700/64 ms, and a 4 minute scan. This will be used to perform tractography and calculate FA. FLAIR data was acquired with $1 \times 1 \times 1$ mm and 6 minute acquisition time, to be used for visualizing and identifying lesions. [17]

We first create an "atlas" of white matter tracts based on healthy individuals. This gives us a baseline of what tract profiles look like in a healthy brain. A population-averaged version of a tract profile can be constructed by averaging DTI data of healthy participants. These white matter tracts can then be warped to each individual, both healthy and MS, and tract profiling will allow us to see how MWF and FA vary along each tract in those subjects. This approach allows us to use the same tracts and locations in each person; performing tractography on each person will result in different fiber bundles. In MS, tractography is unable to follow tracts through lesions, and is not as effective. Using this atlas approach allows for comparison to standardized white matter tracts, in spite of lesion presence.

3.2 Initial registration

Brain MWI, DTI, and FLAIR data from CanProCo is first registered. This allows them to be overlaid so lesions identified in one region of the brain on a FLAIR image can be compared to the same region in the MWF map. These MWF and FA maps were already created from the CanProCo data.

We begin by processing the MWI data. The first step is to extract the 1st and 24th echos from the MWI using the `fslroi` command from the FMRIB Software Library (FSL). The 1st echo is for registration to 3DT1 and the 24th echo for DTI. Next the brain must be extracted from the echos, since some images contain parts of the skull or rest of the head and neck. This allows a version with just the brain to be registered. This is done using the `antsBrainExtraction.sh` command from the Advanced Normalization Tools (ANTs) library, which creates a resulting brain extraction mask. [18] Multiplying the MWF map, 1st echo, and 24th echo by this map using `fslmaths` reduces them to just the brain. FLAIR data already had brain extraction performed in the CanProCo dataset.

Processing DTI data follows largely the same steps. The 1st volume from DTI-B is extracted to be used for image registration. The brain is also extracted from this 1st echo to create the mask, and multiplied to it, removing the skull and everything outside the brain. Now the extracted brain is registered to the 3DT1 brain, generating a series of warps that are used to warp an image to DTI space. This is also done using `antsRegistrationSyN.sh` from the ANTs library.

Since we want to be able to compare MWF and FA values in the same resolution and coordinate space, we will also need to register MWI to DTI space. Registration creates warps to move MWI data to DTI space, and these transforms are now applied to the extracted MWF brain using `antsApplyTransforms` with the `0GenericAffine` file created during registration. FLAIR images undergo the same brain extraction, registration to DTI, and warping process as the MWI data.

The last step is to create a cerebrospinal fluid (CSF) mask. This is necessary so that CSF is avoided when we perform tract profiling. `Atropos` performs K-means clustering to create white matter, grey matter, and CSF masks. In this mask, CSF voxels are labelled as 1, so using `fslmaths` to set an upper and lower threshold of 1 will extract only the CSF regions from the mask. We wish to be able to multiply MWF maps or FA maps by this mask to remove the CSF, so we can again use `fslmaths` invert it so that 0 is non-CSF and 1 is CSF. Fig. 3.1 shows an example of the outcome of this step. A healthy and MS brain are plotted with the FLAIR, MWF, and FA maps. A lesion in the brain appears as a bright spot on the FLAIR image, and is highlighted by the red arrow. Because of image registration, we can directly compare this same region of the brain in the FA and MWF maps to see there appears to be a decrease of those metrics in that same area. This could indicate demyelination and axon damage.

3.3 Tract atlas

The goal of the tract atlas is to create a baseline to which we can compare MS brains to. This allows us to spot irregularities or abnormalities in white matter tracts due to lesions. We create this by averaging over the healthy controls.

Response functions are first created for the healthy controls. In the context of DTI and tractography, response functions capture the characteristics of water diffusion in different types of matter such as white matter or grey matter. Water molecules tend to diffuse along axons in white matter, so the white matter response function can be used to model the primary diffusion direction of different fibers. Response functions for white matter, grey matter, and CSF are made using `dwi2response` using the Dhollander algorithm. They can be averaged over across the healthy controls using `responsemean` from MRtrix3. [19] Next, fiber orientation distribution (FOD) estimates are obtained using `dwi2fod` using the Multi-Shell Multi-Tissue Constrained Spherical Deconvolution (`msmt_csd`) algorithm. This calculates FOD estimates for the three

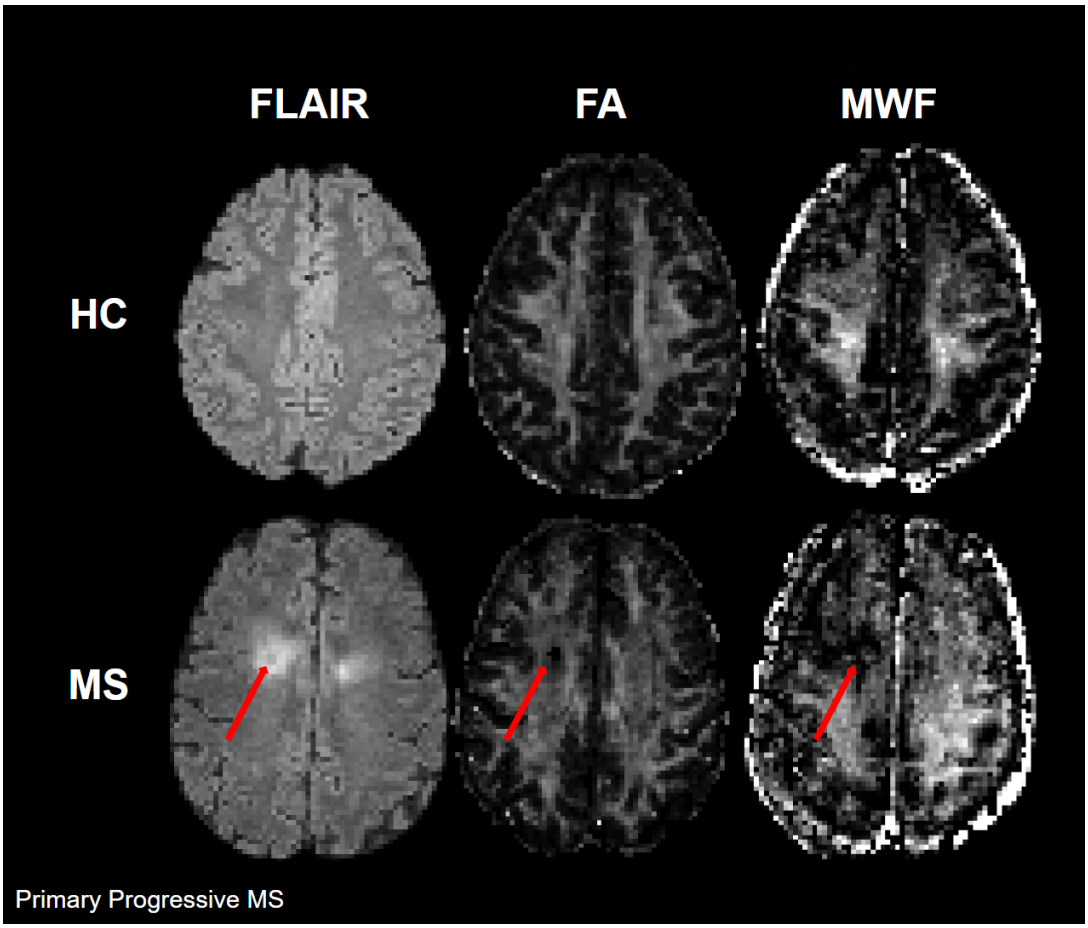

Figure 3.1: FLAIR, FA, and MWF maps for a healthy control and MS brain illustrates the power of image registration for lesion identification. The lesion in the MS brain is indicated by the red arrow. Lesions that appear as bright spots on a FLAIR may also appear on FA and MWF maps as damage in those same regions. Damage levels may vary subject to subject, and even lesion to lesion in the same brain.

types of response means obtained above, which provides information about the likelihood or probability of different fiber directions within a particular voxel. FODs can be used to infer the orientation of nerve fiber bundles in the brain based on diffusion weighted MRI data.

These FODs are then used to create a group-averaged template using `population_template` from MRtrix3. A warp from each healthy control's coordinate system and resolution to the template's is made using `mrregister`. All masks for healthy controls are moved over to template space using `mrtransform`, then combined using `mrmath` into one common template mask. The `sh2peaks` command converts spherical harmonic coefficients of the group-averaged mask into peak directions, which describe the most probable direction of the underlying white matter fibers. The `TractSeg` command from the TractSeg library is then used to create bundle segmentations, ending segmentations, and tract orientation maps based on the converted peaks. Finally, `Tracking` performs tractography on the group template, and outputs the trajectories of the white matter tracts.

3.4 Tractometry for MS

Tractography must also be performed for MS subjects so that we can compare them to the tract atlas. The process shares some similarities to the tract atlas creation. A response mean for the white matter, grey matter, and CSF is made using `dwi2response` for each MS subject. FOD estimates are obtained using `dwi2fod` then normalized with `mtnormalise`. Then each MS subject is registered to the tract atlas using `mrregister` so that we have a way of comparing the same tracts.

The 1st volume from the peaks template is extracted so that it can be used for registration. Warps are created from template space to the native diffusion resolution using `transformcompose` from MRtrix3. This allows us to compare the group-averaged template to each subject, or vice versa. These warps are applied to the ending segmentations and track orientation maps from the tract atlas using `mrtransform` and `tcktransform` respectively. The CSF mask is now applied to the FA and MWF maps by multiplying them, removing the CSF from the brain images.

Tract profiling is performed on the MWF and FA maps for each subject using `Tractometry` from TractSeg. This measures how MWF and FA vary along white matter tracts. Values along the tracts can be compared to the healthy control mean to look for abnormalities.

3.5 Lesion identification and classification

Lesions in the brain appear as bright spots on a FLAIR image. Lesions are identified by looking at the FLAIR images of MS subjects. Different tracts can be overlaid overtop these lesions to see which tracts, if any, pass through that lesion. A list of tracts with lesions in them for each subject can be created by repeating those steps for all the MS subjects.

MWF and FA values can be plotted as a function of position, creating a visualization of the myelin content and axon integrity along the tract. The tract profiles of healthy controls are averaged for each tract, providing a baseline of what a "healthy brain" should look like. The MWF and FA values along a healthy tract will follow a pattern or shape, where certain regions may have higher or lower MWF and FA values. By averaging over the healthy brains, we obtain a mean and 95% confidence interval to which we can compare the MS tract profiles to. Additionally, we can plot all the tracts for a subject, with the ones that pass through a lesion highlighted. Fig. 3.2 contains a few tracts profiles in the corpus callosum for 4 RRMS subjects. Tracts with lesions in them are boxed in red. A plot like this allows us to more easily spot inconsistencies, especially if certain individuals have higher myelin content across the brain overall. This process is repeated for all subjects and tracts of interest. It is important to note MWF and FA values are normalized before plotting, as FA is typically larger than MWF (MWF: typically < 0.2, FA: typically $\sim 0.2 - 0.7$). This allows them to be plotted on the same scale for comparison.

The tract profiles created by tractometry are used to categorize the lesions found. These categories are based on whether MWF or FA is primarily affected, or if both are affected. To categorize lesions, we begin by overlaying a MS tract profile over the healthy average. For example, suppose a region of the tract dips below the 95% confidence interval for MWF, but FA values stay within that 95% confidence interval. We label that lesion as primarily MWF affecting, since it appears only MWF is impacted, and FA remains close to healthy mean values. Below, Table 3.1 summarizes the criteria for each category.

Tracts with lesions in them can also be described by a score representing how far from the healthy mean the tract is. We chose to use the mean average percent error to describe this,

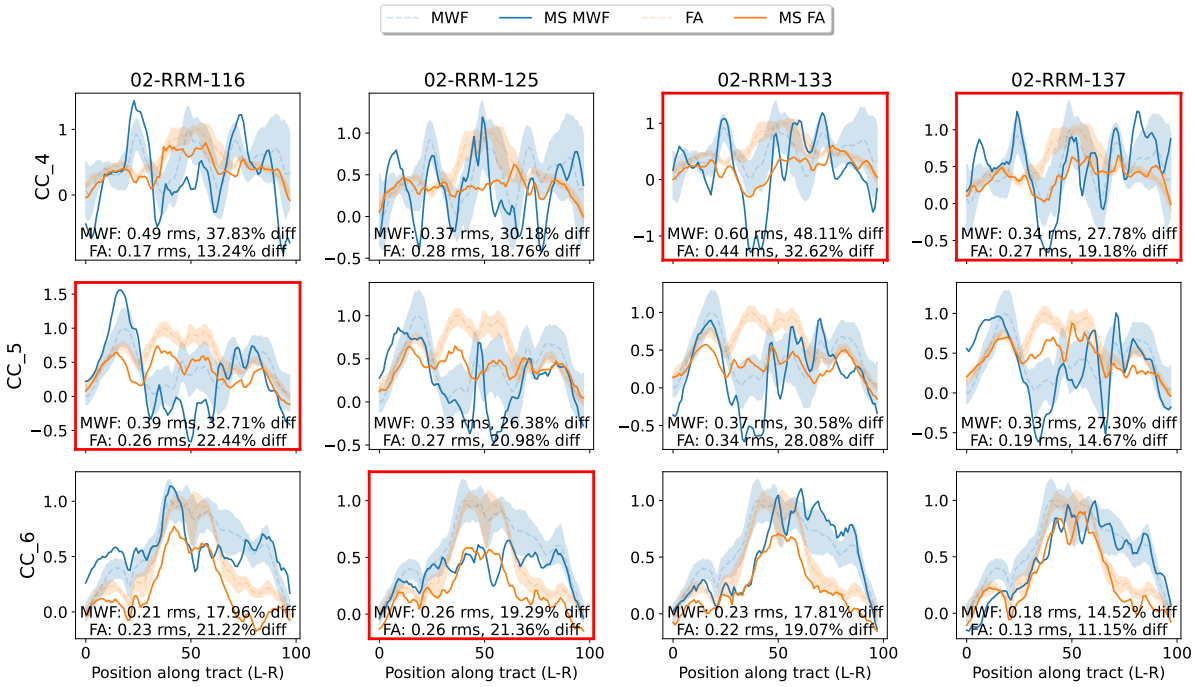

Figure 3.2: Tract profiles of 4 RRMS subjects for portions of the corpus callosum (CC), where red boxes indicate tracts with lesions found on them. This allows us to categorize lesions based on decreases in MWF or FA, as well as compare lesion tracts to tracts where we did not find lesions.

Table 3.1: Categorization criteria

	MWF effect	FA effect
MWF-type lesion	$< 95\%$ CI	–
FA-type lesion	–	$< 95\%$ CI
Both-type lesion	$< 95\%$ CI	$< 95\%$ CI

and Fig. 3.3 illustrates the calculation for it. The absolute value of the difference between the MWF and FA values for the MS versus the healthy control is taken and then averaged. This results in a number that can be used to score how different a MS tract is compared to a healthy brain. It is important to note this metric is calculated off of the unnormalized MWF and FA values, as normalization was for visualization and comparison.

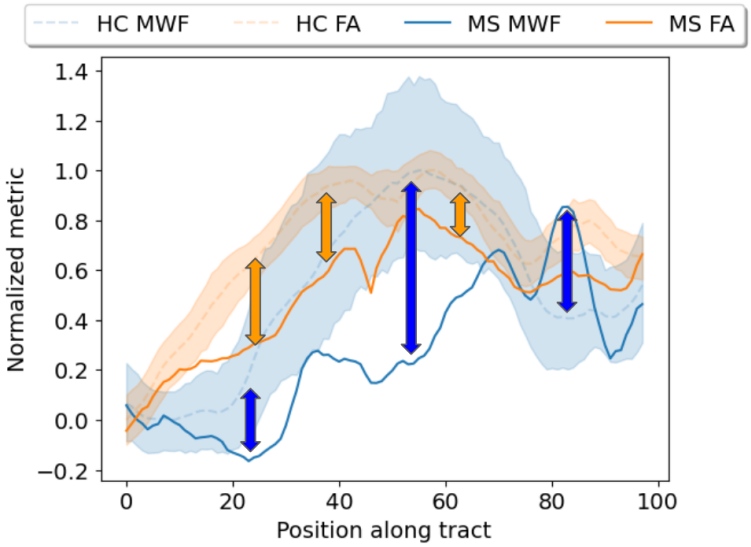

Figure 3.3: Tract profile for a PPMS subject showing MWF and FA values along the tract. FA is plotted in orange and MWF in blue, with the healthy means shown in the corresponding shaded regions. The orange and blue arrows illustrate how mean average percent error (MAPE) is calculated by taking the absolute value of the difference between the tract profile and healthy mean values along the tract, then averaging.

Chapter 4

Results

4.1 Lesion categorization

From the CanProCo data, we have identified three types of lesions based on quantitative MRI metrics: MWF-type, FA-type, and Both-type lesions. Lesions and corresponding tracts were identified in FLAIR images and then classified using their tract profiles.

Tract profiles and the deviation of the MWF or FA from the healthy mean is what determines how a lesion is categorized. In Fig. 4.1, the three identified types of lesions are shown alongside the tract they are on. The MWF-type lesion in the upper left has a distinct drop in MWF values along the whole tract. The MS MWF values are below the blue shaded region, which represents the 95% CI for the healthy mean. This corresponds to a roughly $\sim 40\%$ decrease in that metric. FA values are shown in orange and stay within that orange shaded region, which signifies it is fairly normal. Because of this, the lesion is labelled as a MWF-type lesion. The plot in the upper left is the tract profile for an FA-type lesion. The MWF values in blue remain in or above the 95% CI, while the FA values dip down significantly in the middle of the tract, as well as towards the end. The bottom plot is the tract profile for a Both-type lesion. MWF and FA values exhibit substantial differences compared to the healthy mean. FA is drastically lower across the entire tract. MWF is consistently near the bottom of or below the 95% CI as well.

The number of lesions per category are displayed in Table 4.1 alongside the number of subjects in each type of disease. RIS has the most lesions overall, with RRMS and PPMS having a similar number of lesions. The Both-type lesion is by far the most common with MWF-type lesions being the least common. For RIS and PPMS, the FA-type lesion is more prominent compared to the MWF-type lesion. The opposite is true for RRMS, with the MWF-type lesion appearing more often than the FA-type lesion. Despite PPMS having 4 fewer subjects than RRMS, they have a very similar number of lesions in total.

Table 4.1: Lesion category summary

	MWF-type lesion	FA-type lesion	Both-type lesion	Total
RIS (n = 13)	7	18	34	59
RRMS (n = 15)	8	5	24	37
PPMS (n = 11)	3	14	21	38

Tracts with categorized lesions on them can be visualized by resampling the tracts for their MWF and FA values. This results in images like the ones in Fig. 4.2, 4.3, and 4.4, where the colour of the tract represents the MWF or FA value. As stated above, MWF is a good indicator of myelin content, whereas FA provides information about axon integrity. In a healthy brain, we expect the pattern of the tract to stay similar between individuals. That is, we would expect the same light and darker regions of blue along the tract when comparing MWF values.

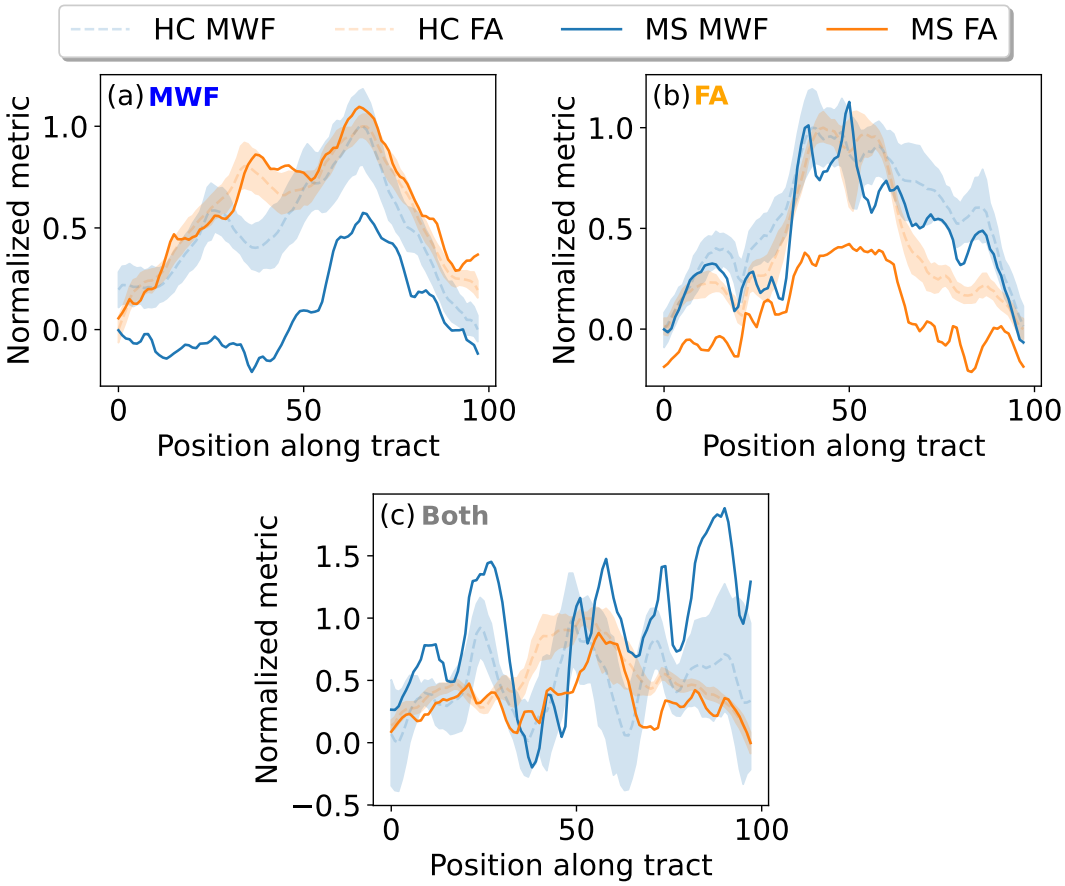

Figure 4.1: Tract profiles for the three categories we identified. (a) MWF-type lesion shows MWF significantly below the healthy average values across the whole tract, and may be primarily myelin damage driven. (b) FA-type lesions show FA decreases in the middle of the tract and may be primarily axon damage driven. (c) Both-type lesions show MWF and FA decreases across the tract, and show signs of damage in both myelin and axon integrity.

In Fig. 4.2 the MWF-type lesion is indicated by the white arrow, with the MWF values plotted in the upper row and FA in the lower row. Around the lesion region we see a significantly darker blue. This suggests there is demyelination in that area, as it is much darker compared to the healthy control brain in that same region. Lesions in the brain are finite in size, and typically smaller than the tract they are on. Despite this lesion only touching a portion of the upper right of the tract, we see there is a region of dark blue surrounding the lesion. This could be the result of downstream damage from the lesion. FA values are fairly similar to the control brain, as the colours, shades, and pattern are comparable.

An FA-type lesion is plotted in Fig. 4.3, with the MWF and FA values plotted in the upper and lower rows respectively. The lesion is again indicated by the white arrow, and is larger than the one in the previous example, as it appears to pass through a large portion of the tract. In the MWF plots, there appears to be no significant differences compared to the healthy control. The left and right parts of the tract are consistent and a similar shade. A more notable discrepancy is seen in the FA plots. The side of the MS tract with the lesion appears spotty, and has dots of much darker orange and red compared to the side without the lesion. Both

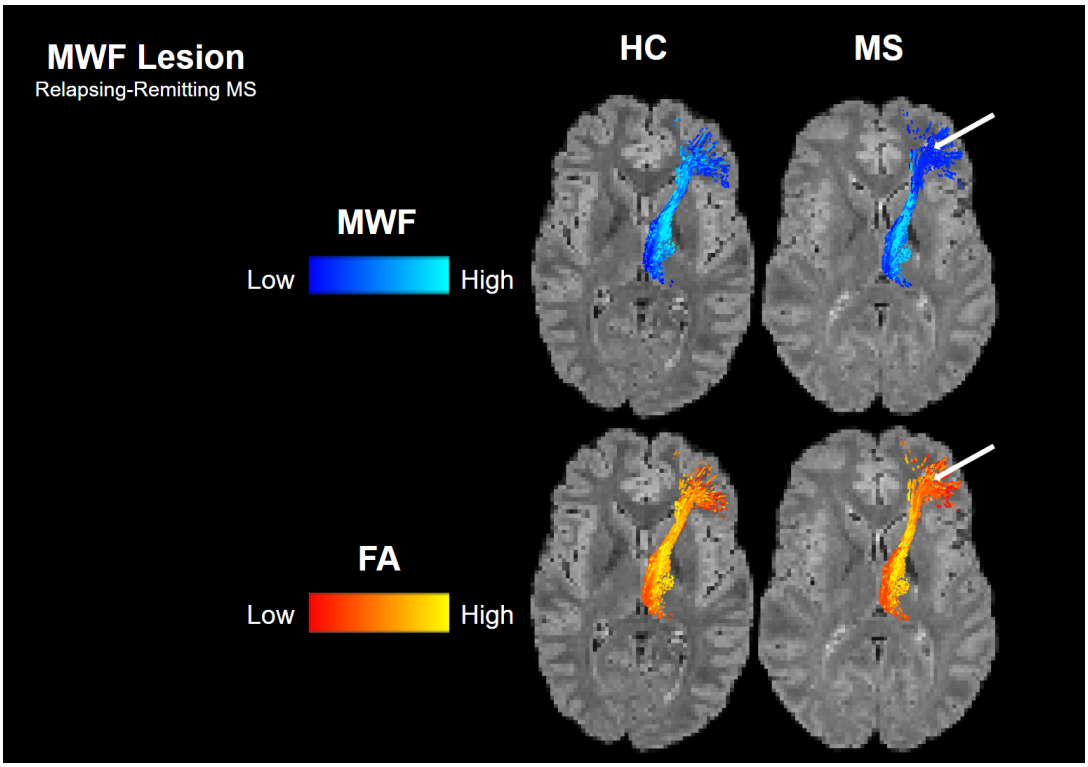

Figure 4.2: White matter tract coloured by MWF and FA values of a MWF-type lesion in a RRMS subject. The lesion is indicated by the white arrow. MWF is decreased compared to the healthy control in the region around the lesion. Parts of the tract not touching the lesion also show signs of decreased myelin, suggesting there may be downstream effects. FA values in the MS tract are comparable to the healthy control.

sides of the tract are a slightly darker shade compared to the healthy control. This could again suggest the lesion is affecting axon integrity across the whole tract, despite only being in one localized area.

An example of a Both-type lesion is shown in Fig. 4.4, where the lesion is again on the right side of the tract. In the MWF plots, the area around the lesion is abnormally darker blue compared to the rest of the tract and to the healthy control. Areas not touching the lesion are also a darker blue, which could again be indication of downstream damage. The other side of the tract appears to be unaffected, as it is much closer in shade and colour to the healthy control. The branches of the tract appear to be darker in the FA plots. Darker orange and spots of red can be seen in some of the branch ends of the tract on both sides. This irregularity appears to be much less pronounced in the FA plots than in the MWF plots.

4.2 Statistical analysis

The mean absolute percent error values for each tract that contained a lesion were calculated and then averaged to obtain Fig. 4.5, which shows a box plot of those averages. The MWF plot contains the MWF-type lesion and the Both-type lesion MAPE values, since Both-type lesions affect MWF as well. Similarly, the FA plot contains FA-type lesions and Both-type lesions. Averages were done by subject grouping, and a distinct separation from the healthy control

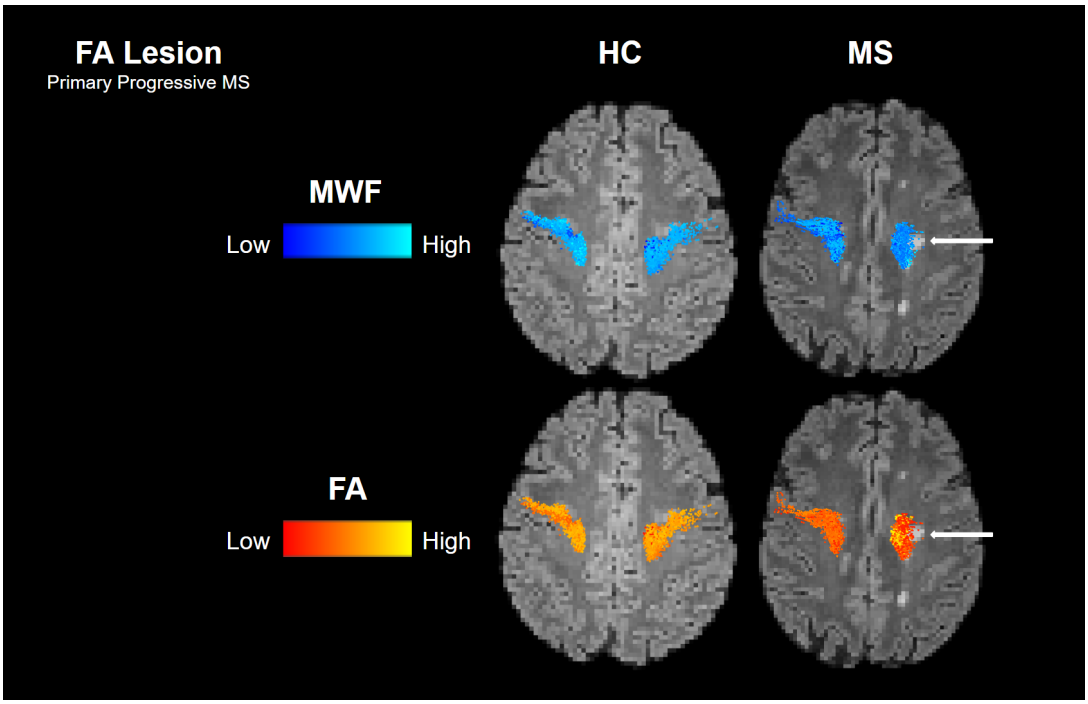

Figure 4.3: White matter tract coloured by MWF and FA values of an FA-type lesion in a RRMS subject. The lesion is indicated by the white arrow. A decrease in FA can be seen in the FA tract near the lesion on the right, and FA appears to be lower overall. MWF appears to be unaffected and similar to the healthy control.

(HC) to the rest of the groups can be seen.

There were statistically significant differences between the HC and RIS, RRMS, and PPMS, but none between RIS, RRMS, and PPMS. ANOVA testing was used to determine if there were statistically significant differences between the HC, RIS, RRMS, and PPMS groups. Table 4.2 summarize those results. The p-values are below 0.05 for all the different metrics. This suggests there are significant differences between these groups, and the large F-value also supports this. To determine which group pairs have these differences, we use Tukey testing, with Tables 4.3 and 4.4 summarizing those results for MWF and FA respectively. The p-values are only lower than 0.05 when comparing PPMS, RRMS, or RIS to the healthy control group. When comparing RRMS, PPMS, and RIS, the p-value are larger than 0.05, indicating these groups are not significantly different. This trend is consistent amongst all three metrics we tried.

Table 4.2: ANOVA results for MWF and FA

	Metric	F-statistic	p-value
MWF	MPE	45.76	1.69×10^{-24}
	MAPE	38.54	3.47×10^{-21}
	RMS	37.61	9.51×10^{-21}
FA	MPE	116.14	2.91×10^{-51}
	MAPE	85.66	5.98×10^{-41}
	RMS	80.79	3.70×10^{-39}

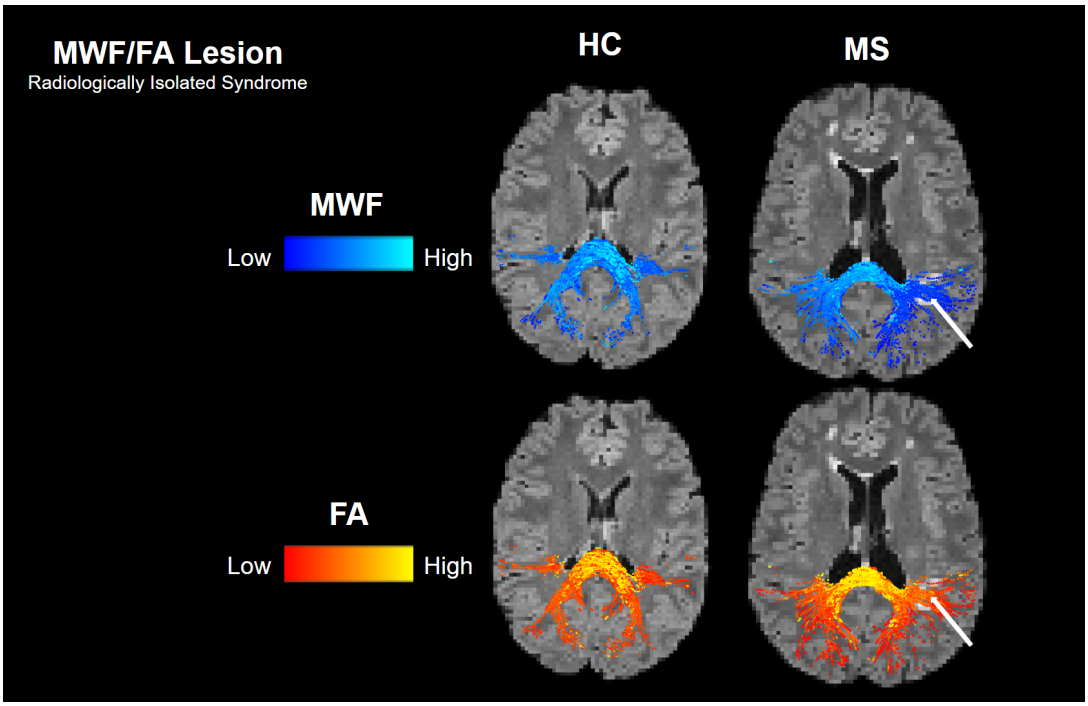

Figure 4.4: White matter tract coloured by MWF and FA values of a Both-type lesion in a RRMS subject. The lesion is indicated by the white arrow. MWF is significantly decreased near the lesion on the right in the MS tract, also showing signs of potential downstream damage. FA is lower near the branches of this tract compared to the healthy control, indicated by the darker orange/red colouring.

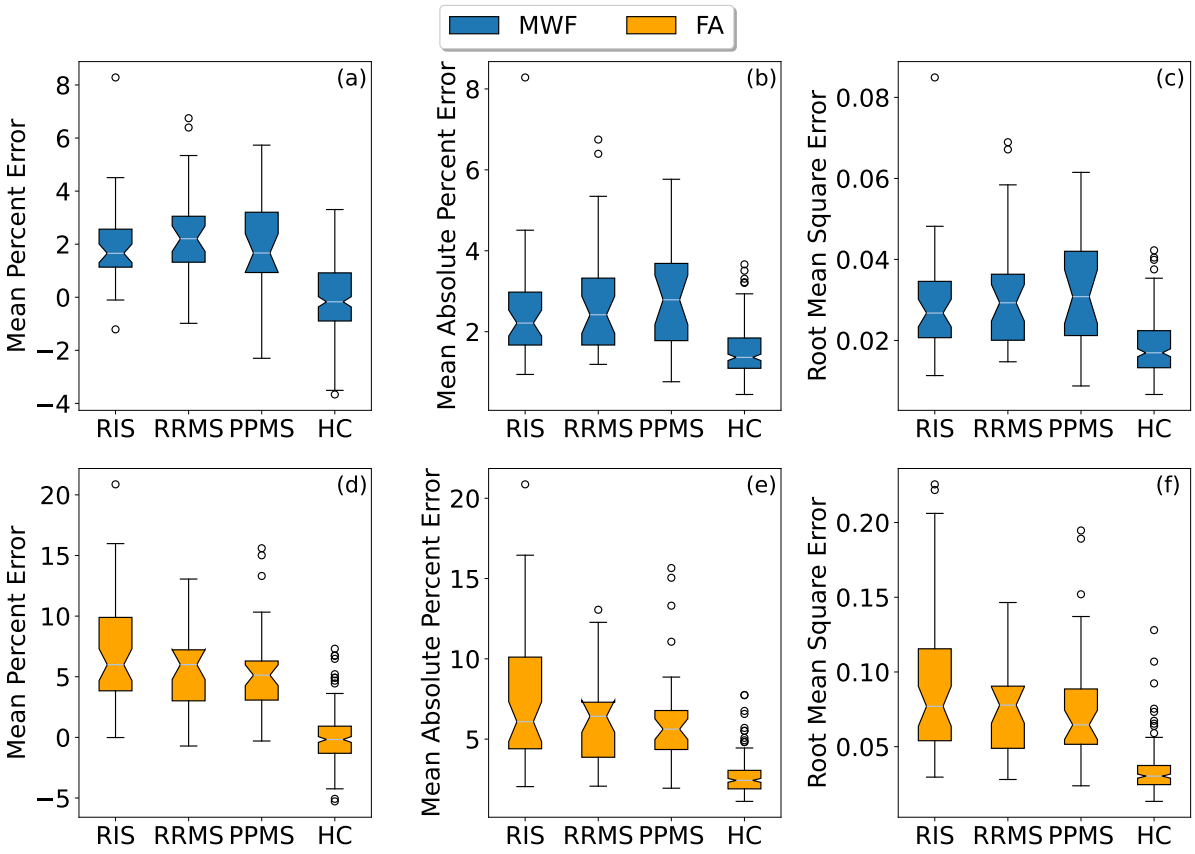

Figure 4.5: Box plots grouped by subject types for various metrics. (a) MWF MPE box plot. (b) MWF MAPE box plot (c) MWF RMS box plot (d) FA MPE box plot (e) FA MAPE box plot (f) FA RMS box plot. All metrics showed statistically significant differences between the HC and the other groups. No metric showed statistically significant differences between RRMs, PPMS, or RIS. It appears RIS has much larger variance in FA damage compared to MWF damage, and is consistent across all three metrics. Similarly, PPMS shows larger variance in MWF than in FA.

Table 4.3: Tukey results for MWF

Metric	Multiple Comparison of Means - Tukey HSD, FWER=0.05						
	Group 1	Group 2	Mean Difference	Lower	Upper	Reject	p-value
MPE	HC	PPMS	1.9327	1.1443	2.7211	True	0.0
	HC	RIS	1.842	1.2178	2.4662	True	0.0
	HC	RRMS	2.3033	1.6092	2.9974	True	0.0
	PPMS	RIS	-0.0907	-1.0324	0.8511	False	0.9946
	PPMS	RRMS	0.3706	-0.6188	1.3601	False	0.768
	RIS	RRMS	0.4613	-0.403	1.3256	False	0.5137
MAPE	HC	PPMS	1.3225	0.8283	1.8167	True	0.0
	HC	RIS	0.9386	0.5474	1.3299	True	0.0
	HC	RRMS	1.2867	0.8516	1.7218	True	0.0
	PPMS	RIS	-0.3839	-0.9742	0.2065	False	0.3362
	PPMS	RRMS	-0.0358	-0.6561	0.5844	False	0.9988
	RIS	RRMS	0.348	-0.1938	0.8898	False	0.3472
RMS	HC	PPMS	0.0141	0.0087	0.0195	True	0.0
	HC	RIS	0.0102	0.0059	0.0144	True	0.0
	HC	RRMS	0.0138	0.0091	0.0186	True	0.0
	PPMS	RIS	-0.0039	-0.0104	0.0025	False	0.3891
	PPMS	RRMS	-0.0003	-0.007	0.0064	False	0.9995
	RIS	RRMS	0.0036	-0.0023	0.0095	False	0.3833

Table 4.4: Tukey results for FA

Metric	Multiple Comparison of Means - Tukey HSD, FWER=0.05						
	Group 1	Group 2	Mean Difference	Lower	Upper	Reject	p-value
MPE	HC	PPMS	5.5425	4.1948	6.8901	True	0.0
	HC	RIS	6.7219	5.5795	7.8644	True	0.0
	HC	RRMS	5.7242	4.2615	7.187	True	0.0
	PPMS	RIS	1.1795	-0.4376	2.7966	False	0.2371
	PPMS	RRMS	0.1818	-1.6755	2.039	False	0.9943
	RIS	RRMS	-0.9977	-2.7119	0.7165	False	0.4369
MAPE	HC	PPMS	3.6636	2.6029	4.7244	True	0.0
	HC	RIS	4.6159	3.7167	5.5152	True	0.0
	HC	RRMS	3.7932	2.6419	4.9445	True	0.0
	PPMS	RIS	0.9523	-0.3205	2.2251	False	0.2166
	PPMS	RRMS	0.1296	-1.3322	1.5914	False	0.9958
	RIS	RRMS	-0.8227	-2.1719	0.5265	False	0.3946
RMS	HC	PPMS	0.044	0.031	0.057	True	0.0
	HC	RIS	0.0561	0.0451	0.0672	True	0.0
	HC	RRMS	0.0423	0.0281	0.0564	True	0.0
	PPMS	RIS	0.0122	-0.0035	0.0278	False	0.1881
	PPMS	RRMS	-0.0017	-0.0197	0.0163	False	0.9948
	RIS	RRMS	-0.0139	-0.0304	0.0027	False	0.1373

Chapter 5

Analysis and Discussion

The current method for categorizing lesions is based on histological staining of post mortem tissue. Three categories currently exist that classify lesions based on the presence or absence of demyelination and inflammatory activity, and the macrophage and microglia distribution. The macrophage is a white blood cell that kills microorganisms and removes dead cells in the body. Microglia is an immune cell responsible for maintenance of CNS tissue, as well as local response to injury or infection. These lesion types are Active, Mixed Active/Inactive, and Inactive lesions. [20]

Active lesions are characterized by the presence of macrophages/microglia throughout the area. They are most commonly observed in patients with RRMS or those with shorter disease durations. These lesions represent the initial appearance of established MS lesions, exhibiting hypercellularity, loss of myelin, and inflammation.

Mixed active/inactive lesions contain macrophages and microglia around the lesion border. They have hypocellular lesion centers and are more common in long-term progressive disease durations (10+ years), and are rare in short-term disease patients. These are characterized by ongoing demyelinating activity and axonal damage. A subset of this category is sometimes referred to as "smoldering" or "slowly expanding" due to a ring of microglia or macrophages creating a degradation product. [21]

Inactive lesions show a lack of macrophages/microglia presence, even fewer compared to normal appearing white matter. There is no rim of microglia or macrophages, and a marked loss of axons may be seen. This type of lesion is dominant in patients with disease durations long-term disease duration, such as exceeding 15 years.

This project's findings align with these categories to a certain extent, and some similarities may be drawn.

Active lesions are characterized by high demyelination and inflammation, which is similar to our MWF-type lesion due to its reduction in MWF, and thus myelin content. It was indeed more common in RRMS. We found similar numbers in RRMS and RIS but less so in PPMS. These were also the least common type of lesion we found, despite existing categorizations labeling it most common in short-term disease duration.

Mixed active/inactive lesions are similar to our Both-type lesions, as this type of lesion is identified by inflammation and ongoing demyelinating activity and axon damage. The decrease in MWF and FA would also suggest demyelination and axon damage. These were the most common type of lesion we found, despite their expected prevalence in long-term progressive disease.

Inactive lesions, marked by significant loss of axons, appear to be similar to our FA-type lesions. A reduction in FA would suggest some damage to axon integrity. These were common in PPMS and RIS but less frequent in RRMS. While this does not agree with inactive lesions being dominant in longer disease durations, this could be attributed to the CanProCo data being taken within 10-15 years of onset rather than 15+ years.

The classifications identified in this project do show some agreement with the existing categorizations, but more research will need to be done to strengthen this connection. The

sample size for this project was small, with only 52 subjects in total, and roughly 10-15 subjects per disease category. Additionally, all participants were patients who had MS onset within 10 years. This may have produced bias in our results, as some lesion types are much more prevalent in long-term disease duration.

There could be many areas of improvement for future work. Lesion categorization in this project was based on finding corresponding lesions and tracts on FLAIR data and using the tract profile to classify them. Since this classification was done manually, there could have been room for human error. Not all tract profiles were easily identifiable as a certain type of lesion. Some tract profiles showed very minute differences from the healthy mean, whereas others showed drastic differences. Individuals who have higher MWF overall also proved challenging to categorize lesions for, as one would have to look for changes in the shape of the curve to find abnormalities. This process of classifying lesions manually can lead to subjectivity and thus error. One area of improvement would be to find a more objective method of identifying and labeling lesions based on these tract profiles. A confidence score was given to each categorization, but we were unable to find a way to incorporate it into the scoring and summary statistics. These scores ranged from 1-3, with a higher number representing a higher confidence in the assigned category. Typically, tracts that had significant decreases in MWF/FA/both across the entire tract were assigned a score of 3. Some tracts had only small regions where MWF/FA would dip slightly below the 95% CI, and may be assigned a score of 1 based on how confident we felt with the lesion classification. Lesions on the extremes with obvious MWF or FA damage ended up with higher confidence scores. On some tracts, it was unclear if the lesion primarily affected MWF, FA, or both; an argument could be made for either category. Ultimately, this categorization process worked well for cases where lesions had clear damage to MWF/FA, and poorly for cases where damage to either was unclear.

Choosing to use the mean absolute percent error of tract profiles as a score could also be reevaluated. Other options such as mean percent error or RMS error were also considered, but MAPE appeared to be the best option. Suppose a subject has consistently higher MWF than the mean, but has a lesion in the middle of the tract. If we were to take MPE, the region above the mean could negate the region below it, resulting in a net zero score. This would incorrectly indicate this tract has no abnormalities, despite the presence of a lesion. MAPE solves this by taking the absolute value of all the differences, quantifying how different a tract is from the mean, rather than how far below the mean it is. RMS was considered but showed similar results to MAPE. A method to consider may be to score only across the region of the tract where the lesion is. However, this runs into problems when the lesion is small, but there is damage across the whole tract. Though MAPE was a useful metric, there may be a more appropriate metric that could reveal more differences between the different disease types.

This project focused on looking at the corpus callosum and superior longitudinal fasciculus due to their known relation to MS-related cognitive impairment. [22] Though some other tracts in and around them were also looked at, this led to some lesions in the brains being overlooked, because no tracts passed through them. A future study may choose to look at a wider range of tracts to capture all lesions in the brain, and provide a more complete look at lesion types. Additionally, as seen in Fig. 3.2, some tracts where we did not find lesions still show signs of myelin and axon damage. Another direction for future work may be to investigate overall damage in the brain due to lesions, and not just in the tracts lesions are present on. Fig. 4.4 shows evidence that supports the idea of downstream damage in tracts, and may be another area for future research.

Chapter 6

Conclusion

Multiple sclerosis exhibits a diverse course of disease progressions and pathological changes. Notably, clinical and cognitive disabilities do not always correlate with the total lesion load. [23] Lesions in MS represent focal areas of demyelination, but can involve more than just demyelination. Different lesion types are known to have different pathologies, and the surrounding tissue also undergoes changes compared to normal appearing white matter. These changes cannot be seen through conventional MRI techniques.

Quantitative MRI offers a more detailed view of microstructural changes within and around lesions. This may aid in assessing the impact of different lesion types on clinical disability. Our objective is to investigate whether specific lesion types contribute to clinical disability, and this project is the first step towards that goal. Our focus is on categorizing lesions in vivo using 2 quantitative metrics - MWF, representing myelin content, and FA, representing axon integrity. We analyze how these metrics vary across white matter tracts and within lesions.

Through this, we have identified three lesion categories, which roughly align with existing histological classifications, although some discrepancies exist. Future work can expand on this approach by looking at more data, as well as the longitudinal CanProCo data spanning 4 years. We would be able to see if there are changes in lesion types over time and how they may correspond to clinical or cognitive disability.

Bibliography

[1] Vijay P B Grover, Joshua M Tognarelli, Mary M E Crossey, I Jane Cox, Simon D Taylor-Robinson, and Mark J W McPhail. Magnetic resonance imaging: Principles and techniques: Lessons for clinicians. *J Clin Exp Hepatol*, 5(3):246–255, Aug 2015.

[2] Alex L MacKay and Cornelia Laule. Magnetic resonance of myelin water: An in vivo marker for myelin. *Brain Plast*, 2(1):71–91, Dec 2016.

[3] Wint Yan Aung, Soe Mar, and Tammie Ls Benzinger. Diffusion tensor MRI as a biomarker in axonal and myelin damage. *Imaging Med*, 5(5):427–440, Oct 2013.

[4] M. T. Wallin, W. J. Culpepper, E. Nichols, Z. A. Bhutta, T. T. Gebrehiwot, S. I. Hay, I. A. Khalil, K. J. Krohn, X. Liang, M. Naghavi, A. H. Mokdad, Nixon M. R., R. C. Reiner, B. Sartorius, M. Smith, R. Topor-Madry, A. Werdecker, T. Vos, V. L. Feigin, and C. J. L. Murray. Global, regional, and national burden of multiple sclerosis 1990-2016: a systematic analysis for the global burden of disease study 2016. *Lancet Neurol.*, 18(3):269–285, Jan 2019.

[5] H. Lassmann. Multiple sclerosis pathology. *Cold Spring Harb Perspect Med.*, 8, MAR 2018.

[6] Jiwon Oh, Nathalie Arbour, Fabrizio Giuliani, Melanie Guenette, Shannon Kolind, Larry Lynd, Ruth Ann Marrie, Luanne M Metz, Scott B Patten, Alexandre Prat, Alice Schabas, Penelope Smyth, Roger Tam, Anthony Traboulsee, and V Wee Yong. The canadian prospective cohort study to understand progression in multiple sclerosis. *BMC Neurology*, 21(1):418, Oct 2021.

[7] D. J. Werring, D. Brassat, A. G. Droogan, C. A. Clark, M. R. Symms, G. J Barker, D. G. MacManus, A. J. Thompson, and D. H. Miller. The pathogenesis of lesions and normal-appearing white matter changes in multiple sclerosis: A serial diffusion MRI study. *Brain*, 123(8):1667–1676, 08 2000.

[8] Abi Berger. Magnetic resonance imaging. *BMJ*, 324(7328):35, Jan 2002.

[9] Bernhard Blümich. The incredible shrinking scanner. *Sci Am*, 299(5):92–6, 98, Nov 2008.

[10] Yves Gossuin1, Aline Hocq1, Pierre Gillis1, and Vuong Quoc Lam1. Physics of magnetic resonance imaging: from spin to pixe. *J. Phys. D: Appl. Phys.*, 43, May 2010.

[11] C Laule, E Leung, D K B Lis, A L Traboulsee, D W Paty, A L MacKay, and G R W Moore. Myelin water imaging in multiple sclerosis: quantitative correlations with histopathology. *Mult Scler*, 12(6):747–753, Dec 2006.

[12] A MacKay, K Whittall, J Adler, D Li, D Paty, and D Graeb. In vivo visualization of myelin water in brain by magnetic resonance. *Magn Reson Med*, 31(6):673–677, Jun 1994.

[13] José M Soares, Paulo Marques, Victor Alves, and Nuno Sousa. A hitchhiker's guide to diffusion tensor imaging. *Front Neurosci*, 7:31, Mar 2013.

[14] Andrew L Alexander, Jee Eun Lee, Mariana Lazar, and Aaron S Field. Diffusion tensor imaging of the brain. *Neurotherapeutics*, 4(3):316–329, Jul 2007.

[15] Jakob Wasserthal, Peter Neher, and Klaus H. Maier-Hein. Tractseg - fast and accurate white matter tract segmentation. *NeuroImage*, 183:239–253, 2018.

[16] John Kruper, Jason D Yeatman, Adam Richie-Halford, David Bloom, Mareike Grotheer, Sendy Caffarra, Gregory Kiar, Iliana I Karipidis, Ethan Roy, Bramsh Q Chandio, Eleftherios Garyfallidis, and Ariel Rokem. Evaluating the reliability of human brain white matter tractometry. *Apert Neuro*, 1(1), Nov 2021.

[17] Jiwon Oh, Nathalie Arbour, Fabrizio Giuliani, Melanie Guenette, Shannon Kolind, Larry Lynd, Ruth Ann Marrie, Luanne M. Metz, Scott B. Patten, Alexandre Prat, Alice Schabas, Penelope Smyth, Roger Tam, Anthony Traboulsee, and V. Wee Yong. The canadian prospective cohort study to understand progression in multiple sclerosis (canproco): rationale, aims, and study design. *BMC Neurology*, 21(1):418, 2021.

[18] Brian B. Avants, Nicholas J. Tustison, Michael Stauffer, Gang Song, Baohua Wu, and James C. Gee. The insight toolkit image registration framework. *Frontiers in Neuroinformatics*, 8, 2014.

[19] J-Donald Tournier, Robert Smith, David Raffelt, Rami Tabbara, Thijs Dhollander, Maximilian Pietsch, Daan Christiaens, Ben Jeurissen, Chun-Hung Yeh, and Alan Connelly. Mrtrix3: A fast, flexible and open software framework for medical image processing and visualisation. *NeuroImage*, 202:116137, 2019.

[20] Tanja Kuhlmann, Samuel Ludwin, Alexandre Prat, Jack Antel, Wolfgang Brück, and Hans Lassmann. An updated histological classification system for multiple sclerosis lesions. *Acta Neuropathologica*, 133(1):13–24, 2017.

[21] Douglas L Arnold, Shibeshih Belachew, Arie R Gafson, Laura Gaetano, Corrado Bernasconi, and Colm Elliott. Slowly expanding lesions are a marker of progressive ms – no. *Multiple Sclerosis Journal*, 27(11):1681–1683, 2021. PMID: 34474615.

[22] Shawna Abel, Irene Vavasour, Lisa Eunyoung Lee, Poljanka Johnson, Stephen Ristow, Nathalie Ackermans, Jillian Chan, Helen Cross, Cornelia Laule, Adam Dvorak, Alice Schabas, Enedino Hernández-Torres, Roger Tam, Annie J. Kuan, Sarah A. Morrow, Jeffrey Wilken, Alexander Rauscher, Virender Bhan, Ana-Luiza Sayao, Virginia Devonshire, David K. B. Li, Robert Carruthers, Anthony Traboulsee, and Shannon H. Kolind. Associations Between Findings From Myelin Water Imaging and Cognitive Performance Among Individuals With Multiple Sclerosis. *JAMA Network Open*, 3(9):e2014220–e2014220, 09 2020.

[23] Amjad I AlTokhis, Abrar AlAmrani, Abdulmajeed Alotaibi, Anna Podlasek, and Cris S Constantinescu. Magnetic resonance imaging as a prognostic disability marker in clinically isolated syndrome and multiple sclerosis: A systematic review and meta-analysis. *Diagnostics (Basel)*, 12(2):270, 2022. PMID: 35204361.